Dilation Dependent Matched Filtering for SAR Signal Processing

The relative motion between radar and targets in large time-bandwidth product synthetic aperture radar (SAR) induces serious dilation in the received signal. To process the received signal with serious dilation, a new technique called dilation dependent matched filtering (DDMF) is proposed to combine with the two-dimensional space frequency interpolation wavefront reconstruction (SFIWR) method. The DDMF-SFIWR method can effectively eliminate the impact of dilation when the illuminated area is relatively small, as verified by simulations and acoustic experiments.

I. INTRODUCTION

The most distinguished feature of synthetic aperture radar (SAR) is the motion of antenna. This motion can be further characterized into three categories [2]: 1) motion occurring between successive transmitted pulses, 2) motion occurring during transmission and reception of a pulse, 3) motion occurring in the interval between transmission and reception of a pulse. In current SAR systems, since the pulse duration is very short and the bandwidth is not so large, the last two categories of motion are ignored in the signal processing stage. However, for large time-bandwidth product signals, the antenna motion during and between transmission and reception cannot be ignored anymore. While the motion during transmission has no impact on the received signal, the motion during reception and between transmission and reception will induce serious dilation in the received signal [12, 5, 7], especially when the speed of the antenna is very high such as for spaceborne radars [3, 4]. The amount of dilation is dependent on the product of time duration, bandwidth, and speed of antenna [12, 7]. It is shown in [7] that for SAR with large time-bandwidth product signals, the dilation can cause serious distortions in the reconstructed images using conventional signal processing methods. On the other hand, large time-bandwidth product signals are important for high resolution SAR. Actually, large bandwidth leads to high range resolution [2, 7, 10], and long duration waveforms result in low probability of interception (LPI) and other advantages [1, 7].

Manuscript received April 5, 2003; revised July 1, 2004; released for publication November 17, 2004.

IEEE Log No. T-AES/41/2/849047.

Refereeing of this contribution was handled by P. Lombardo.

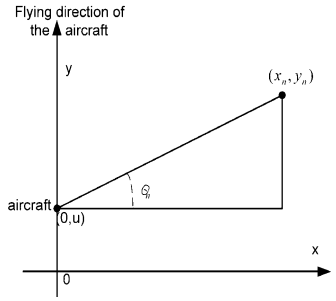

Fig. 1. Airborne SAR model.

Therefore, it is expected that large time-bandwidth product signals will be widely used in future SAR systems.

In order to process the received signal with serious dilation, a "wideband compensation" method and a "narrowband compensation" method have been proposed in [7]. Although the two methods can improve the reconstructed SAR images, both of them have drawbacks: they are constrained by the accuracy of the approximation methods, and need a rough estimation of target locations and reflectivities. When the received signal is extremely distorted or some targets are closely located, the two methods are not effective. A new method called dilation dependent matched filtering (DDMF) is proposed here to overcome the drawbacks of the compensation methods. Simulations and real world acoustic SAR experiments are presented to demonstrate the superiority of the proposed method.

II. DILATION DEPENDENT MATCHED FILTERING

An airborne SAR is described by Fig. 1. The aircraft is moving along the y axis and its location is at $(0,u)$, where $u \in [-L,L]$. The length of the synthetic aperture is $2L$. We assume that the aircraft is moving along a straight line at a constant velocity v and transmits the same signal $p(t)$ at many different locations. The propagation speed of the signal is c. Although the following discussions can be extended to any type of targets, we only consider the case of point-targets here for simplicity. The illuminated targets are located at (x_n,y_n) $(n = 1,2,\ldots,N)$, where x_n is the range and y_n is the cross-range. For simplicity, all the targets are assumed motionless. From Fig. 1, we see that

$$\sin\theta_n = \frac{y_n - u}{r_n} \tag{1}$$

where θ_n is the squint angle and r_n is the distance between the radar and the nth target

$$r_n = \sqrt{x_n^2 + (y_n - u)^2}. \tag{2}$$

Since the aircraft is moving at speed v along axis y, the target at (x_n,y_n) has a relative radial speed $v\sin\theta_n$. Therefore, the received signal reflected by the target at

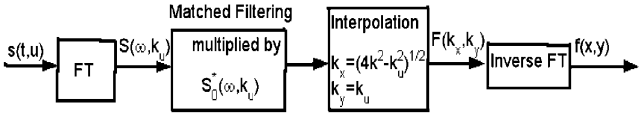

Fig. 2. Block diagram of SFIWR.

(x_n, y_n) is [11, 12]

$$s_n(t,u) = \sigma_n p(\lambda_n(t-\tau_n)) \tag{3}$$

where σ_n is the reflectivity of the target at (x_n, y_n) (σ_n includes the propagation phase and is assumed to be invariant in radar frequency),

$$\lambda_n = \frac{c + v\sin\theta_n}{c - v\sin\theta_n}, \qquad \tau_n = \frac{2r_n}{c}. \tag{4}$$

The received signal reflected from the illuminated area becomes

$$s(t,u) = \sum_{n=1}^{N} s_n(t,u) = \sum_{n=1}^{N} \sigma_n p(\lambda_n(t-\tau_n)). \tag{5}$$

In current SAR practice, the dilation (scale factor) λ_n is ignored in signal processing, that is, the received signal is assumed to be [2, 10]

$$\bar{s}(t,u) = \sum_{n=1}^{N} \bar{s}_n(t,u) = \sum_{n=1}^{N} \sigma_n p(t-\tau_n). \tag{6}$$

It is shown in [7] that such a simplification (assumption) may lead to poor results when the bandwidth B of the transmitted waveform is very large and the time duration T of the waveform is long. Noticing that the relative radial speed here is related to target and platform locations, we know that, unlike in range radar, the "narrowband condition" [9, 12, 7] should be stated as

$$TBv\sin\theta_n \le 0.1c. \tag{7}$$

In current SAR practice, this condition is usually satisfied and therefore the dilation can be ignored. In the following, a new method is proposed to combat the dilation effect when (7) is violated.

The two-dimensional (2D) space frequency interpolation wavefront reconstruction method (SFIWR) [10] is an efficient method for SAR signal processing. The block diagram of SFIWR is shown in Fig. 2 (in the figure, $k = \omega/c$ is the wavenumber). A crucial step in the SFIWR is the 2D matched filtering with the following filtering function

$$s_0(t,u) = p\left(t - \frac{2R}{c}\right) \tag{8}$$

whose Fourier transform is denoted by $S_0(\omega, k_u)$, where

$$R = \sqrt{X_c^2 + (Y_c - u)^2}. \tag{9}$$

If the product of dilation λ_n and the time duration of the transmitted signal is large, this matched filter obviously does not match the received signal. A filter that includes the dilation λ_n would be better. Unfortunately, since λ_n depends on the locations of targets which are unknown, it is impossible to include λ_n in the matched filtering. However, in some cases, the radar swath is a small region, that is, the interested targets are located in a small region centered at (X_c, Y_c). Then λ_n will not vary significantly in the whole region and it is possible to approximate it by a target-independent value. In fact, based on the first-order Taylor expansion

$$\sin\theta_n - \sin\theta \approx -\frac{X_c(Y_c - u)}{R^3}(x_n - X_c) + \frac{X_c^2}{R^3}(y_n - X_c)$$

where

$$\sin\theta = \frac{Y_c - u}{R} \tag{10}$$

we have, approximately,

$$|\sin\theta_n - \sin\theta| \le \frac{1}{R}(|x_n - X_c| + |y_n - Y_c|). \tag{11}$$

If X_c and Y_c are relatively large and (x_n, y_n) is near (X_c, Y_c), which is likely the case for spotlight SAR, we have $\sin\theta_n \approx \sin\theta$. Therefore,

$$\lambda_n \approx \lambda_u = \frac{c + v\sin\theta}{c - v\sin\theta}. \tag{12}$$

Since λ_u only depends on the speed v, the location parameter of aircraft u and the known target center (X_c, Y_c), it can be computed. The received signal is thus approximated by

$$s(t,u) \approx \sum_{n=1}^{N} \sigma_n p(\lambda_u(t-\tau_n)). \tag{13}$$

Approximation (12) may not be applicable to stripmap SAR where the illuminated area is usually quite large and therefore some targets may be far away from the target center. To illustrate the accuracy of the approximations, we have computed the relative mean square error (RMSE) of (13) and (6) compared with the real received signal (5). Table I gives the results, where the radar parameters are in Table II, only one target at $(X_c + 0.4X_0, Y_c + 0.5Y_0)$ is assumed, and the Frank code is used as the transmitted signal. Obviously the approximation (13) is much more accurate than the approximation (6).

TABLE I
Error of Approximations

v (km/s)	RMSE of (6) (dB)	RMSE of (13) (dB)
4	−16.91	−31.79
40	−7.02	−21.29
400	1.25	−11.78

From (13), it is obvious that

$$\bar{s}_0(t,u) = p\left(\lambda_u\left(t - \frac{2R}{c}\right)\right) \tag{14}$$

can be used for matched filtering. We call this DDMF. Combining the DDMF with the 2D SFIWR [10],

TABLE II
Simulation Parameters

Parameter	Symbol	Value	Units
Speed of signal	c	3×10^8	m/s
Bandwidth	B	200	MHz
Carrier frequency	f_c	200	MHz
Pulse length	T	1	μs
Synthetic aperture	$2L$	400	m
Center range	X_c	200	m
Range swath	$2X_0$	60	m
Center cross-range	Y_c	300	m
Cross-range extent	$2Y_0$	120	m

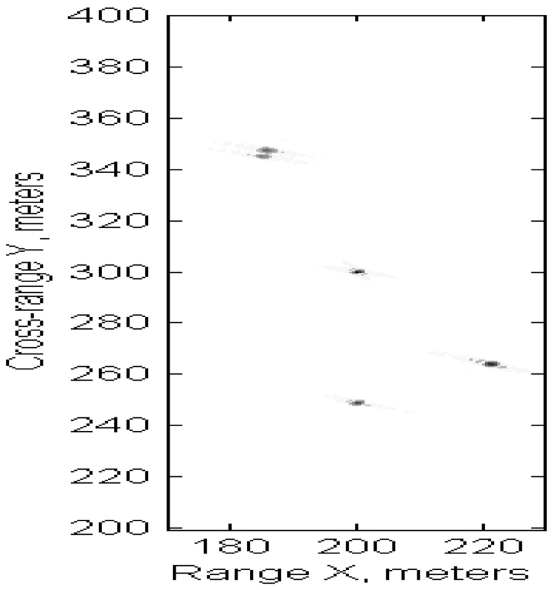

Fig. 3(a). Reconstructed SAR image (Frank code) (ideal case).

we have a new algorithm for large time-bandwidth product SAR signal processing described in the following.

ALGORITHM 1 *DDMF-SFIWR.*

Step 1 *Compute the Fourier transform (by fast Fourier transform (FFT) algorithm) of sampled functions* $s(t,u)$ *and* $\bar{s}_0(t,u)$ *and let the results be* $S(\omega,\eta)$ *and* $\bar{S}_0(\omega,\eta)$*, respectively.*

Step 2 *Implement the DDMF,* $G(\omega,\eta) = S(\omega,\eta)\bar{S}_0(\omega,\eta)$.

Step 3 *Convert* $G(\omega,\eta)$ *into* $F(K_x,K_y) = G\left((c\sqrt{K_x^2+K_y^2}/2),K_y\right)$*, where a 2D space frequency interpolation method is used to obtain an evenly spaced data set of* $F(K_x,K_y)$ *[10].*

Step 4 *Compute the inverse Fourier transform of sampled* $F(K_x,K_y)$ *to get* $f(x,y)$*, the target function.*

III. SIMULATIONS AND COMPARISONS

We have developed Matlab codes for the DDMF-SFIWR method based on the programs attached to [10]. The basic parameters for the simulations are listed in Table II. In order to save simulation time, we choose the central frequency f_c to be low. Since the method is only valid for small region, the range swath and cross-range extent are assumed to be relatively small. Different targets are allowed to have different radar cross-sections and no threshold is used in the plots.

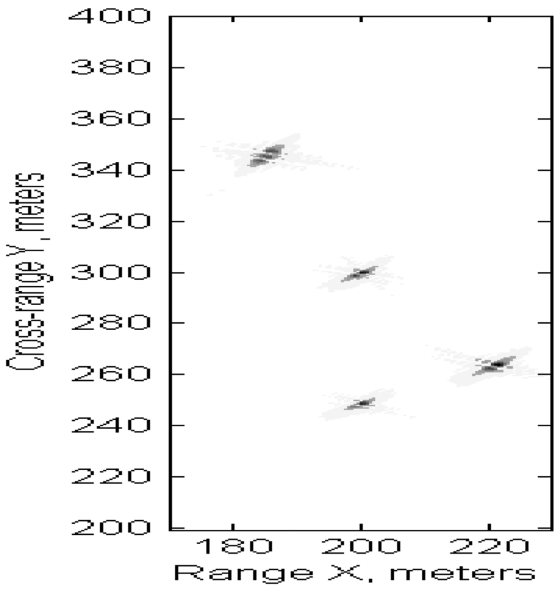

Fig. 3(b). Reconstructed SAR image (Frank code) (v = 400 km/s).

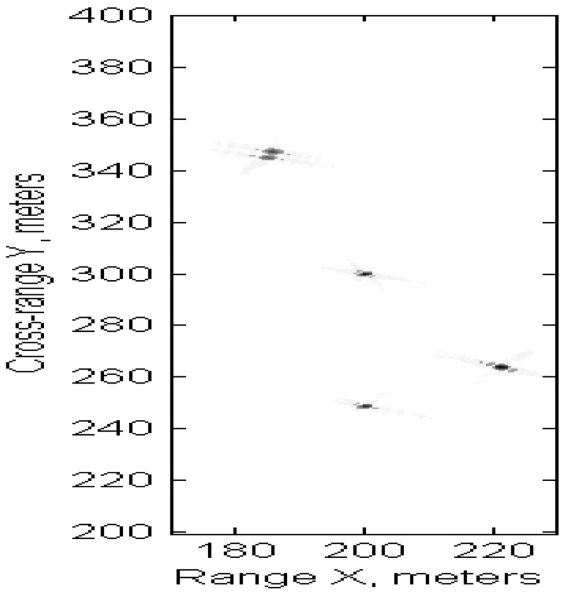

Fig. 3(c). SAR image by presented method (Frank code) (v = 400 km/s).

A. Reconstructed SAR Images

Assume that there are five separate point-targets. Figs. 3(a)–3(c) are the reconstructed SAR images by different methods, where the transmitted signals are Frank codes of length 100. In Fig. 3(a), the ideal undilated received signal given by (6) is used. In Fig. 3(b), the speed is v = 400 km/s and the received signal is given by (5). The SFIWR method [10] is

TABLE III
Comparison of Resolutions (Frank Code)

Method	Deviation (m)	Range Resolution (m)	SL1 (dB)	Cross Resolution (m)	SL2 (dB)
ideal	(0, −0.0061)	0.9353	−14.51	1.6816	−10.81
DDMF	(0, −0.0061)	1.2334	−14.26	1.6816	−7.89
direct	(0, −0.0061)	1.2334	−1.56	1.6816	−7.24

used to obtain these two figures. Note that a matched filter (8) ignoring the dilation effect is used here. In Fig. 3(c), the speed is also $v = 400$ km/s and the received signal is also given by (5), but the presented DDMF-SFIWR method (14) is used. We can see that the image in Fig. 3(b) is distorted compared with Fig. 3(a). In particular, the two closely located targets cannot be discriminated anymore. However, Fig. 3(c) is nearly the same as Fig. 3(a) and we can still distinguish the two closely located targets. We can also use the RMSE to evaluate the differences. The RMSE between two SAR images $f_1(i,j)$ and $f_2(i,j)$ is defined by

$$\text{RMSE} = \sqrt{\frac{\sum_{i=1}^{I}\sum_{j=1}^{J}|f_1(i,j)-f_2(i,j)|^2}{\sum_{i=1}^{I}\sum_{j=1}^{J}|f_1(i,j)|^2}}.$$

The RMSE between the two images in Figs. 3(a) and 3(b) is −17.9 dB, while that between the two images in Figs. 3(a) and 3(c) is −24.1 dB. Thus, a considerable improvement has been achieved by using the DDMF-SFIWR method.

It should be pointed out that in this example, T and B are not so large but v is impractically big. This is of course not the case in practice. Rather, they are used to save time and memory in simulations. It has been proved in [7] that the impact of waveform distortion caused by the dilation remains almost unchanged if we keep TBv constant while letting v be very large and TB be relatively small. The platform speed of a spaceborne radar at altitude around 800 km is about 7.5 km/s. So, for an X-band (8–12 GHz) spaceborne radar with bandwidth 300 MHz (this is a possible choice in the future, see [4, Table 1]), if $T = 0.04$ ms, TBv will be larger than the one associated with Figs. 3(b) and 3(c). Hence, we can imagine that the same scene will occur as in Figs. 3(b) and 3(c). Because of the very large memory and computational power required, it is very difficult to do simulations for this case. Similarly, the same scene will occur as in Figs. 3(b) and 3(c) if $T = 0.4$ ms, $B = 1$ GHz and $v = 200$ m/s (this may become practical for SAR applications in the near future).

B. Point Spread Function and Resolution

The target function in the spatial domain is

$$f(x,y) = \sum_n \sigma_n f_n(x - x_n, y - y_n) \tag{15}$$

where $f_n(x,y)$ is the point spread function (PSF) of target n. In spotlight SAR systems, the PSF $f_n(x,y)$ varies with the coordinates of the nth target [10]. The shape of the PSF depends on the location of the target as well as the radar parameters such as bandwidth and carrier frequency. In the narrowband case, the PSF is like a separable 2D sinc function in a coordinate system which is a rotation of the original coordinates by an angle $\alpha_n = \arctan(y_n/x_n)$ [10]. In the wideband case, however, the PSF cannot be approximated by a 2D sinc pattern. Its shape is much more complex and hence very difficult to be characterized analytically.

In the 1D case, we usually use the width or the 3 dB width of the mainlobe of the PSF as the resolution. In the 2D case, however, we have to consider range resolution and cross-range resolution, respectively. That is, we need to choose two directions in the 2D plane to consider the widths of the corresponding PSFs along the directions. As discussed above, in spotlight SAR systems, we could choose the x axis rotated by an angle α_n as one direction and a 90 deg rotation of this line as the other direction. In the following, we use the 3 dB widths of mainlobes of the PSFs in these two directions as the range resolution and the cross-range resolution, respectively. The sidelobe of a 1D signal means the ratio of the second largest value to peak value. No weighting is used for sidelobe suppression. Since we are only interested in the resolutions, we assume that there is only one target. As we use the dilation of the center point of the illuminated region in the DDMF-SFIWR, it is obvious that the method would produce better resolutions for targets near the center than for those near the border. The average case should be for targets between the center and the borders. Therefore, we assume that the only target is located at $(X_c + 0.4X_0, Y_c + 0.5Y_0)$.

In Table III, the radar parameters are the same as those for Figs. 3(a)–3(c), except that there is now only one target located at (212, 330). In the tables, "ideal" stands for the case when v is very small compared with c; "DDMF" for DDMF-SFIWR; "direct" for directly applying the SFIWR. The column "deviation" shows the deviations of the estimated target locations from the theoretical ones. SL1 and SL2 are used for range and cross-range sidelobes, respectively. Note that the above convention is also adopted in the remainder of this paper.

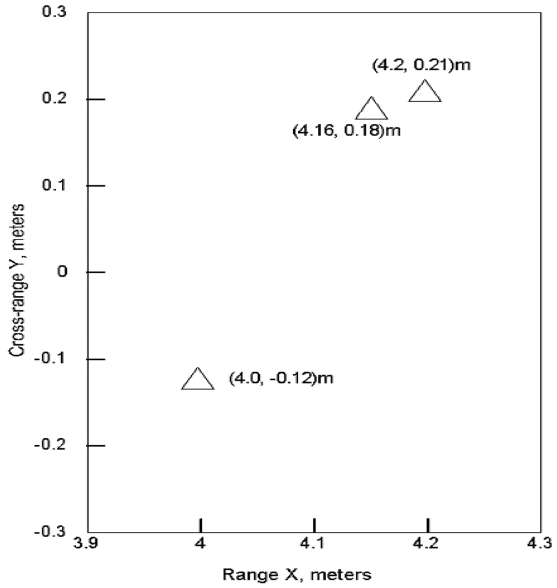

Fig. 4(a). Exp 1. Target positions.

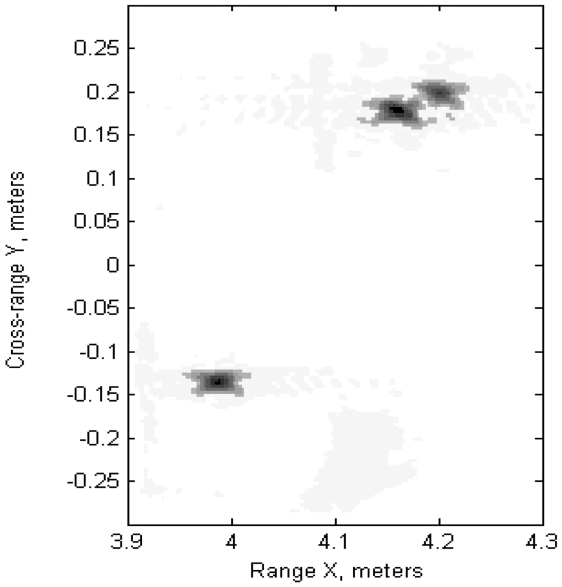

Fig. 4(b). Exp 1. Direct method.

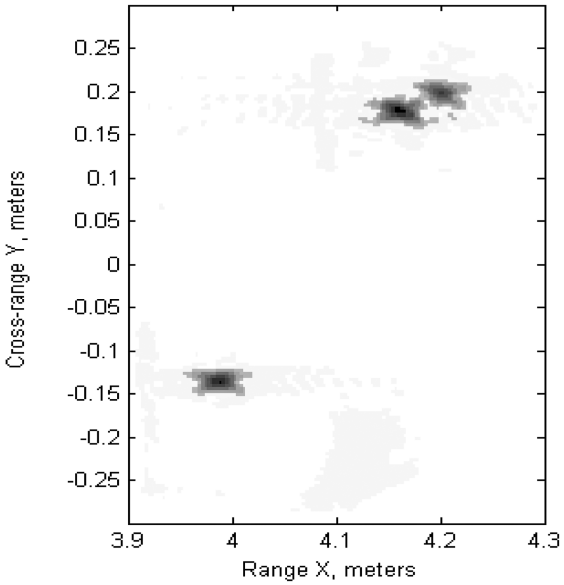

Fig. 4(c). Exp 1. Wideband compensation method.

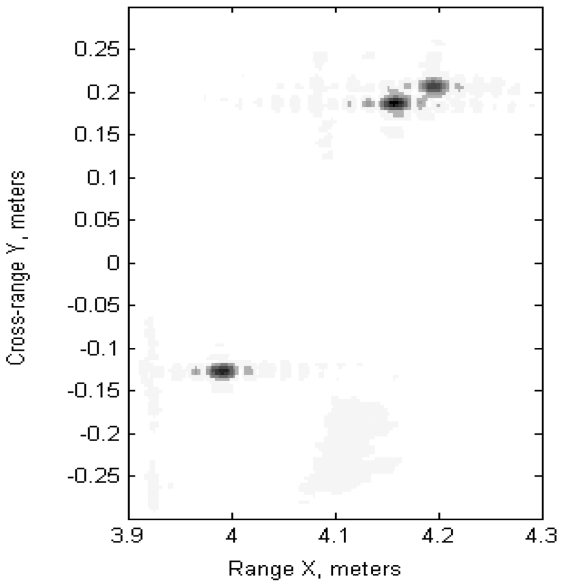

Fig. 4(d). Exp 1. DDMF-SFIWR method.

TABLE IV
Parameters for Experiments

Parameter	Symbol	Exp1	Exp2	Units
Speed of signal	c	351	351	m/s
Platform velocity	v	0.12	0.24	m/s
Bandwidth	B	10	18	kHz
Carrier frequency	f_c	50	50	kHz
Pulse length	T	150	80	ms
Synthetic aperture	$2L$	2	2	m
Center range	X_c	4.1	3.8	m
Range swath	$2X_0$	0.4	0.4	m
Center cross-range	Y_c	0	2.6	m
Cross-range extent	$2Y_0$	0.6	0.6	m

We have carried out extensive simulations under different parameter settings. We cannot show all of them here due to page limits. In general, simulations show that the DDMF-SFIWR method can always improve the imaging in spotlight SAR no matter how the radar parameters and targets parameters are. The improvement varies with radar and target parameters. The smaller the size of target region or the closer the target to the center, the more the improvement we obtain. Furthermore, like other matched filtering methods, the DDMF-SFIWR method is robust to white noise.

C. Comparisons with Compensation Methods

The basic idea of the "wideband compensation" and "narrowband compensation" in [7] is: getting an approximation of the undilated received signal by

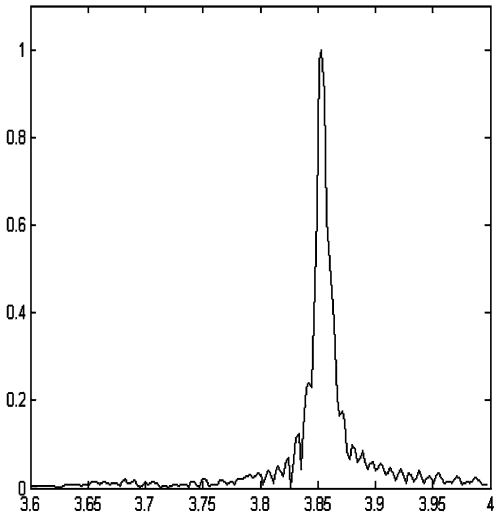

Fig. 5(a). Exp 2. Range point spread function (conventional method).

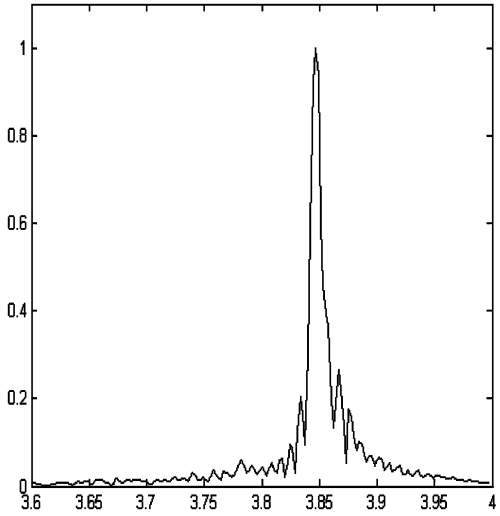

Fig. 5(c). Exp 2. Range point spread function (wideband compensation).

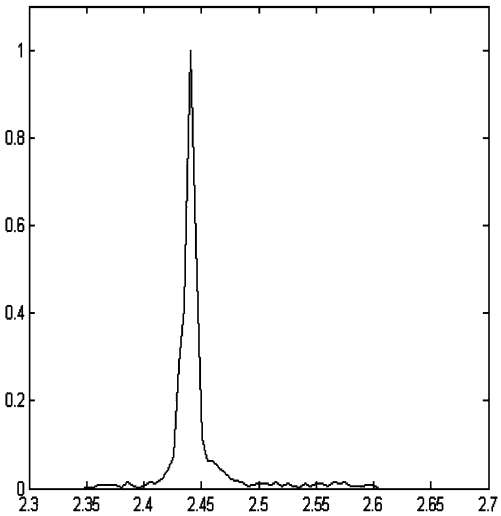

Fig. 5(b). Exp. 2. Cross-range point spread function (conventional method).

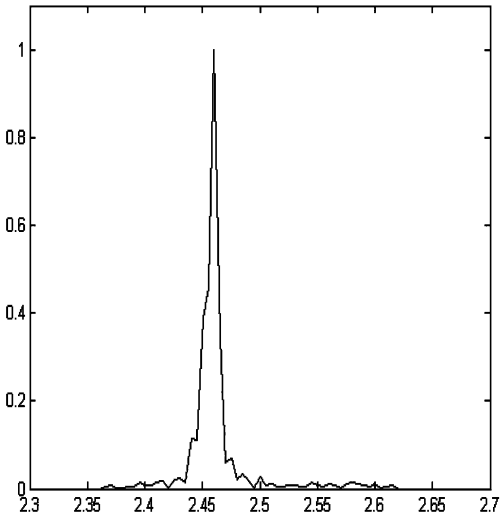

Fig. 5(d). Exp 2. Cross-range point spread function (wideband compensation).

using the estimations of target parameters and then reconstructing the SAR image by using a conventional method. The difference between the two methods is that wideband compensation estimates the dilation while narrowband compensation estimates the Doppler frequency. The main problems of them are: 1) it is difficult to get the estimations of target parameters when the received signal is extremely distorted or some targets are closely located, and 2) even if we have the estimations of target parameters, there are still errors in the approximated undilated received signal due to the accuracy of the approximation methods. For example, in Fig. 3(b), due to the dilation the two closely located targets cannot be distinguished and therefore it is very difficult (or even impossible) to get accurate estimations of target parameters. As a result, we would most probably get the wrong target parameters. However, the DDMF-SFIWR method can separate the two targets (see Fig. 3(c)). Furthermore, it has the same complexity as SFIWR, and is always applicable whether the dilation is serious or not. If the dilation is not serious, as in current SAR applications, the method will provide no much better but never worse performance. The compensation methods require additional computations.

The only disadvantage of the DDMF-SFIWR method is that it is effective only when the size of the illuminated region is small such as for spotlight SAR.

IV. ACOUSTIC SAR EXPERIMENTS

Acoustic SAR experiments were conducted in an anechoic acoustic chamber at the DSO National Laboratories, Singapore. A linear motion control stage is used to simulate the linear flight path of a SAR

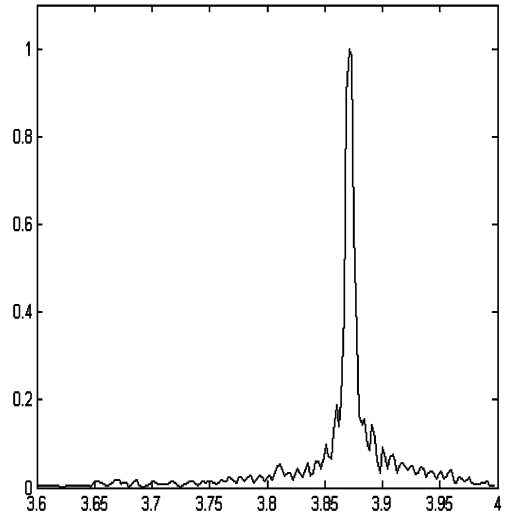

Fig. 5(e). Exp. 2. Range point spread function (DDMF-SFIWR).

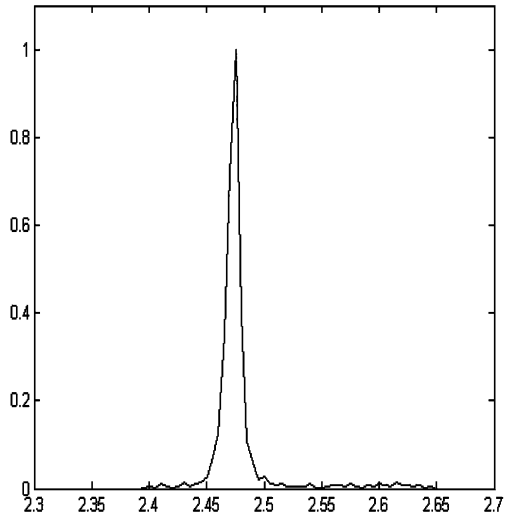

Fig. 5(f). Exp 2. Cross-range point spread function (DDMF-SFIWR).

system. During the motion, linear FM chirp pulses are transmitted from the transmitter, an ultrasonic transducer. The returned signals are received with the receiver, a measurement microphone which is placed together with the transmitter. The physical dimensions and available equipment of the acoustic chamber impose some constraints on the experimental parameters. In particular, the platform velocity v is limited due to the motion control equipment which is designed to move very slowly. Despite these constraints, the time-bandwidth product can be made large enough so that the waveform dilation cannot be ignored. We conducted two experiments. The parameters used for the two experiments are given in Table IV. Note that c is the speed of sound rather than the speed of light here.

For the first experiment, $TBv = 0.15 \times 10^4 \times 0.12 \approx 0.51c$. Hence, the narrowband condition (7) is violated and the waveform dilation should not be ignored. The scene contained three point targets. Two of them were positioned as close as possible to each other. The positions of the targets are shown in Fig. 4(a). Fig. 4(b) shows the reconstructed SAR image by directly applying the SFIWR. The dilation effect is clearly visible. Fig. 4(c) shows the reconstructed SAR image by the wideband compensation method. Comparing Fig. 4(c) with Fig. 4(b), there does not appear to be any improvement. Fig. 4(d) shows the reconstructed SAR image by the DDMF-SFIWR method. There is a considerable improvement compared with Fig. 4(b) and Fig. 4(c). The two closely-placed targets are now resolved clearly.

In the second experiment we considered only a single point-target located at (3.87, 2.47) (m). From Table IV, $TBv = 0.08 \times 1.8 \times 10^4 \times 0.24 \approx 0.98c$. Again, the narrowband condition is violated. Figs. 5(a), 5(c), and 5(e) show the range PSFs by the SFIWR [10], the wideband compensation method [7], and the DDMF-SFIWR method, respectively, while Figs. 5(b), 5(d), and 5(f) show the cross-range PSFs by them, respectively. It is clear that the DDMF-SFIWR method outperforms the existing methods in terms of range resolution and sidelobe level. Although cross-range resolutions are comparable for all the three methods, the DDMF-SFIWR method produces the lowest first sidelobe. Furthermore, it is interesting to note that the estimated target location by the DDMF-SFIWR method is much more accurate than the ones by the other two methods.

The acoustic SAR experiments have demonstrated the following. 1) Conventional SAR processing methods, such as the SFIWR [10], fail for sufficiently large time-bandwidth product signals. 2) The wideband compensation method [7] may not be applicable for closely placed targets. 3) The DDMF-SFIWR method can effectively overcome the dilation effect for small illuminated areas, such as the ones considered in our acoustic SAR experiments.

V. CONCLUSIONS

A new technique called DDMF has been proposed. Simulations and acoustic SAR experiments have shown that the proposed method can improve the quality of the simulated SAR images greatly when the illuminated area is relatively small. We believe that this method can be used for future large time-bandwidth product airborne SAR systems and spaceborne SAR systems, especially for spotlight mode SAR.

ACKNOWLEDGMENT

The authors would like to thank Adrian Yap, Chye Hwang Yen, and Wee Kok Pek of DSO National Laboratories, Singapore for helpful discussions.

YONGHONG ZENG
School of Electrical and Electronic Engineering
Nanyang Technological University
Singapore
and
Institute for Infocomm Research
Singapore

ZHIPING LIN
GUOAN BI
School of Electrical and Electronic Engineering
Nanyang Technological University
Block S2, Nanyang Avenue
Singapore 639798
Republic of Singapore
Email: (ezplin@ntu.edu.sg)

JOCELYN YEO
SHANGUO LU
DSO National Laboratories
Singapore

REFERENCES

[1] Burgos-Garcia, M., Sanmartin-Jara, J., Perez-Martiniz, F., and Retamosa, J. A.
Radar sensor using low probability of interception SS-FH signals.
IEEE Aerospace and Electronic Systems Magazine, **15** (2000), 23–28.

[2] Carrara, W., Goodman, R. S., and Majewski, R. M.
Spotlight Synthetic Aperture Radar: Signal Processing Algorithms.
Norwood, MA: Artech House, 1995.

[3] Elachi, C.
Space imaging radar in planetary exploration and earth observation.
AIAA Journal, **39**, 4 (2001), 553–563.

[4] Huneycutt, B., and Zuzek, J.
Frequency use and needs of spaceborne active sensors.
In *Proceedings of IEEE International Geoscience and Remote Sensing Symposium* (IGARSS), *Vol. 6*, 2000, 2457–2463.

[5] Jin, Q., and Wong, K. M.
The estimation of time delay and Doppler stretch of wideband signals.
IEEE Transactions on Signal Processing, **43**, 4 (1995), 904–916.

[6] Klugmann, D.
A compact 94-GHz FM-CW Doppler cloud radar using semiconductor devices for power generation.
In *Proceedings of IEEE International Geoscience and Remote Sensing Symposium* (IGARSS), *Vol. 5*, 2000, 1801–1803.

[7] Lin, Z., Zeng, Y., Bi, G., and Yeo, J.
Signal processing for large bandwidth and long duration SAR.
Multidimensional System and Signal Processing, **14**, 1–3 (2003), 119–137.

[8] Noda, S., Inomata, K., Watanabe, M., Fukae, T., and Tobioka, M.
A millimeter-wave radar for train application.
In *Proceedings of IEEE International Conference on Vehicle Electronics Conference* (IVEC), *Vol. 1*, 1999, 153–158.

[9] Rihaczek, A. W.
Principles of High Resolution Radar.
New York: McGraw-Hill, 1969.

[10] Soumekh, M.
Synthetic Aperture Radar Signal Processing with MATLAB Algorithms.
New York: Wiley, 1999.

[11] Van Trees, H. L.
Detection, Estimation and Modulation Theory.
New York: Wiley, 2001, 238–242.

[12] Weiss, L. G.
Wavelets and wideband correlation processing.
IEEE Signal Processing Magazine, **11** (1994), 13–32.

Comparison of Low Angle Radar Clutter Models

Three low angle clutter models, the compound-K, the noncentral gamma-gamma (NCGG), both of which model speckle, and the Weibull distributions are compared. The derivations of the first two densities are surprisingly similar, differing on only one critical point. The compound-K assumes that the Gaussian random variables that are the input to the square law detector have zero means, while the NCGG assumes that the Gaussian random variables have nonzero means. The compound-K must then assume that it is the output variance that is fluctuating to produce speckle, while the NCGG assumes that it is the noncentrality parameter, resulting from the addition of the nonzero means, that is fluctuating. The difference in the resulting models is significant.

The Weibull density has long been used to model clutter successfully, and it too will be considered for comparison, but its use is not based upon a physically motivated development. Rather, its use is based on comparisons of clutter output densities being well matched by the Weibull density with appropriate parameters.

I. INTRODUCTION

Three models for low angle clutter are considered: the compound-K [1–4], the noncentral gamma-gamma (NCGG) [5], and the Weibull [6] densities. The use of the first two is based on physical motivation, while the use of the Weibull is based on its matching the clutter output power density.

Although the compound-K is usually developed in terms of the output amplitude level, we will compare these models based on output power levels, which simply correspond to the square of the amplitudes.

Manuscript received December 5, 2003; revised May 31 and September 27, 2004; released for publication December 18, 2004.

IEEE Log No. T-AES/41/2/849048.

Refereeing of this contribution was handled by E. S. Chornoboy.